Prediction of Hydroplaning Risk of Truck on Roadways

FINAL REPORT
January 2018

Submitted by:

Hao Wang
Associate Professor

Yangmin Ding
Graduate Research Assistant

Center for Advanced Infrastructure and Transportation (CAIT)
Rutgers, The State University of New Jersey,
Piscataway, NJ, 08854

External Project Manager
Susan Gresavage
Manager, Pavement and Drainage Management Unit
New Jersey Department of Transportation

In cooperation with

Rutgers, The State University of New Jersey
And
State of New Jersey
Department of Transportation
And
U.S. Department of Transportation
Federal Highway Administration

Disclaimer Statement

The contents of this report reflect the views of the authors, who are responsible for the facts and the accuracy of the information presented herein. This document is disseminated under the sponsorship of the Department of Transportation, University Transportation Centers Program, in the interest of information exchange. The U.S. Government assumes no liability for the contents or use thereof.

The Center for Advanced Infrastructure and Transportation (CAIT) is a National UTC Consortium led by Rutgers, The State University. Members of the consortium are the University of Delaware, Utah State University, Columbia University, New Jersey Institute of Technology, Princeton University, University of Texas at El Paso, Virginia Polytechnic Institute, and University of South Florida. The Center is funded by the U.S. Department of Transportation.

TECHNICAL REPORT STANDARD TITLE PAGE

1. Report No.	2. Government Accession No.	3. Recipient's Catalog No.
CAIT-UTC-NC46		

4. Title and Subtitle	5. Report Date
Prediction of Hydroplaning Risk of Truck on Roadways	January 2018
	6. Performing Organization Code CAIT/Rutgers University

7. Author(s)	8. Performing Organization Report No.
Hao Wang, PhD and Yangmin Ding	CAIT-UTC-NC46

9. Performing Organization Name and Address	10. Work Unit No.
Center for Advanced Infrastructure and Transportation Rutgers, The State University of New Jersey 100 Brett Road,Piscataway, NJ 08854	11. Contract or Grant No. DTRT13-G-UTC28

12. Sponsoring Agency Name and Address	13. Type of Report and Period Covered
Center for Advanced Infrastructure and Transportation Rutgers, The State University of New Jersey 100 Brett Road, Piscataway, NJ 08854	Final Report 10/01/2016 – 12/31/2017
	14. Sponsoring Agency Code

15. Supplementary Notes

U.S. Department of Transportation/OST-R
1200 New Jersey Avenue, SE
Washington, DC 20590-0001

16. Abstract

The risk of hydroplaning is one of major safety concerns at rainy weather condition for both travel public and highway agencies. Most previous studies have focused on analysis of hydroplaning for passenger car tires while giving limited importance to truck tires. This study aimed to investigate hydroplaning risk of truck tires and compare hydroplaning speeds of different tire configurations using three-dimensional (3D) fluid-structure interaction models. The validation of hydroplaning simulation model was performed against the field test results from existing literature. The results show that the wide-base 445 tire provides better safety performance than the conventional wide-base 425 tire and dual tire assembly with 11R22.5 tire under wet weather condition. The hydroplaning potential increases with the increase of water film thickness on pavement surface. On the other hand, the high wheel load or high tire inflation pressure positively increases hydroplaning speed. In addition, the analysis results demonstrate that the truck tire under sliding condition has the higher hydroplaning risks than the tire under free rolling condition. These factors should be considered together when developing safety improvement countermeasures for driving safety.

17. Key Words	18. Distribution Statement
hydroplaning; truck tire; fluid-structure interaction, water film, sliding, load and pressure	

19. Security Classification (of this report)	20. Security Classification (of this page)	21. No. of Pages	22. Price
Unclassified	Unclassified	Total #38	

Form DOT F 1700.7 (8-69)

Table of Contents

Section 1: Introduction 1
1.1 Problem Statement 1
1.2 Objective and Scope 2
Section 2: Development of Finite Element Tire Model 4
2.1 Descriptions of Tire Model 4
2.2 Validation of tire model with tire deflections 6
Section 3: Fluid-Structure interaction models 8
3.1 Fluid Domains 8
3.2 Solid Domains 9
3.3 Coupling of the Equations for Fluid and Structure 10
Section 4: Hydroplaning Model 12
4.1 Tire Hydroplaning Model 12
4.2 Validation of Hydroplaning Model 14
Section 5: Results and Discussions 17
5.1 Effect of tire configuration on hydroplaning 17
5.2 Effect of water film thickness on hydroplaning 20
5.3 Effect of wheel load on hydroplaning 22
5.4 Effect of tire inflation pressure on hydroplaning 24
5.5 Effect of tire sliding on hydroplaning 26
5.6 Conclusions 28
References 30

List of Figures

Figure 1 Flowchart of analysis methodology used in this study. 3
Figure 2 Truck tire models used in the analysis. 6
Figure 3 Comparisons between measured and predicted deflections. 7
Figure 4 Mesh configuration of fluid model. 14
Figure 5 Truck tire hydroplaning model with contact force variation. 14
Figure 6 Illustration of water flow into tire contact patch for (a) single 11R22.5 tire, (b) wide-base 425 tire, and (b) wide-base 445 tire at 96 km/h. 19
Figure 7 Tire-pavement contact force variation during hydroplaning process. 20
Figure 8 Water film thicknesses along drainage path length at different conditions. 21
Figure 9 Effect of water film thickness on hydroplaning speed. 22
Figure 10 Effect of wheel load on hydroplaning speed. 23
Figure 11 Illustration of water penetration into tire contact patch at various vertical load for wide-base 445 tire. 24
Figure 12 Effect of tire inflation pressure on hydroplaning speed. 25
Figure 13 Illustration of water penetration into tire contact patch at various tire pressure levels for wide-base 445 tire. 26
Figure 14 Hydroplaning speeds of wide-base 445 tire under free rolling and locked-wheel conditions. 27
Figure 15 Illustration of water flow into contact patch of wide-base 445 tire under free rolling and sliding conditions. 28

List of Tables

Table 1 . Groove dimensions for truck tires 4
Table 2 Hydroplaning Speeds for 425/65R22.5 and 11R22.5 Tires 16

Section 1: Introduction

1.1 Problem Statement

As one of key issues for safe driving on wet pavement, hydroplaning occurs when a tire loses contact with water-covered road surface by water pressure that builds up with the increasing vehicle speed (Stocker *et al.* 1974, Veith 1983). Many experimental and numerical studies have been conducted to predict hydroplaning speed for passenger car tires and aircraft tires (Harrin 1958, Horne and Dreher 1963, Sinnamon 1974, Ong et al. 2015; Fwa and Ong 2007). The studies on hydroplaning by various researchers have revealed valuable knowledge on the mechanisms and factors affecting tire hydroplaning. Several empirical equations for determining hydroplaning speed have been widely employed (Harrin 1958, Gallaway 1979). However, these studies focused on the hydroplaning risk on passenger car tires and very few attentions have been given to hydroplaning on truck tire, especially on wide-base tires.

It has been found that lightly loaded truck tires possess higher hydroplaning potential than full loaded trucks, indicating that the wheel load may have significant impact on truck tire hydroplaning (Ivey 1984). An early experimental study compared the hydroplaning risk between wide-base tire and conventional dual tires, which showed that the wide-base tire was less susceptible to hydroplaning than dual tires (Tielking 1992). Analytical simulation models have been developed to study hydroplaning behaviour of a bias ply truck tires under different inflation pressure

levels, footprint aspect ratios, wheel loads, and water-film thicknesses. The results further confirm that truck tires do hydroplane and truck hydroplaning can even occur within the range of normal highway operating speeds (Ong and Fwa 2008).

The trucking industry recently has developed new generation of wide-base tire technology for the purposes of improving fuel efficiency of vehicle operations and minimizing tire wear. The use of wide-base tires is receiving considerable attention due to economic and environmental benefits, particularly for the new generation of wide-base tires (wide-base 445 and 455) (Al-Qadi and Elseifi 2007). A number of studies were conducted to investigate pavement damage mechanisms induced by different truck tire configurations using theoretical modelling and field instrumentations. These studies concluded that the new wide-base 445 or 455 tire could cause greater or less pavement damage potential than the dual-tire assembly, depending on pavement structure and failure mechanism (Wang and Al-Qadi 2011; Al-Qadi and Wang 2012).

The aforementioned studies focus on the impact of wide-base tires on pavement damage. However, researches on the impact of wide-base tires on safety, especially the driving stability under inclement weather condition is quite limited. Therefore, it is desired to investigate the safety performance of wide-base tires, such as hydroplaning risk on flooded pavement surface at rainy condition.

1.2 Objective and Scope

This study aims to analyse hydroplaning potential of different tire configurations using three-dimensional (3-D) finite element simulations based on fluid-structure interaction in ABAQUS 10.0. The hydroplaning risk of two wide-base tires (425/65R22.5 and 445/50R22.5) is analysed as compared to conventional tire (11R22.5) used in dual tire assembly. The effects of water film thickness, wheel load and inflation pressure, operation condition on hydroplaning speeds of truck tires were also investigated. Figure 1 shows the flowchart of analysis methodology used in this study.

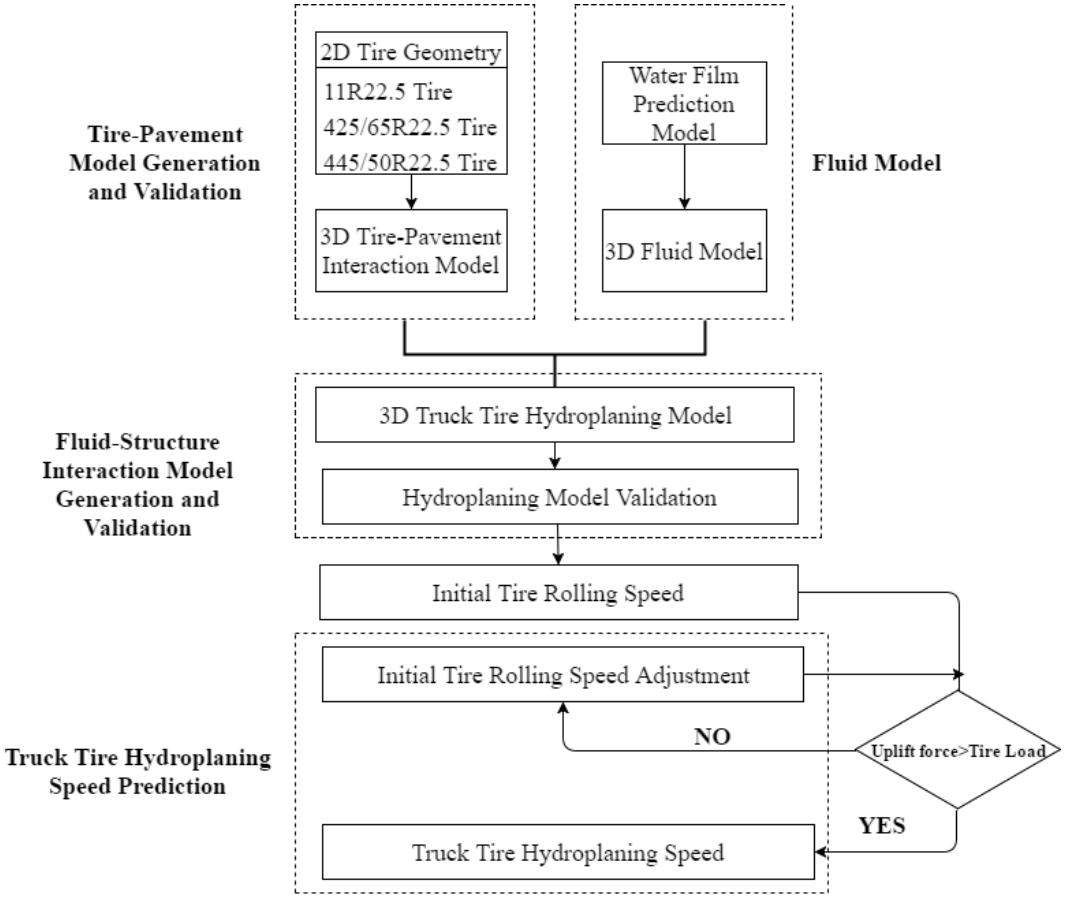

Figure 1 Flowchart of analysis methodology used in this study.

Section 2: Development of Finite Element Tire Model

2.1 Descriptions of Tire Model

Three truck tire configurations were considered in the analysis, including 11R22.5, 425/60R22.5, and 445/50R22.5. The nomenclature of tires usually includes three tire dimensions and types of tire in the form of AAA/BBXCC.C. The first number (AAA) is the tire width from wall to wall in mm or inch, the second number (BB) is the sidewall height given as a percentage of the tire width. The letter (X) indicates the type of tire (radial or bias ply). The third number (CC.C) is the tire rim diameter in inches. For example, the 11 or 425/60 gives the section width and aspect ratio. "R" is for radial tires. The 22.5 is the wheel diameter. The longitudinal groove patterns of tires are simulated. 5Based on the information from tire manufactures, the groove dimensions for the truck tires used in this study are presented in Table 1.

Table 1 . Groove dimensions for truck tires

Type of Truck Tire	Number of grooves	Groove depth (mm)	Groove width (mm)
11R22.5	4	15	8.1
425/65R22.5	5	15	8.1
445/50R22.5	7	22	8.4

In tire hydroplaning analysis, the focus is global contact between tire and water or pavement surface, not the local deformation of tire components. The rainwater flow and the resulting contact forces are more sensitive to the tread block geometry and the

total kinetic energy of tire (Cho *et al*. 2006). In the tire model, the reinforced rubber part is modelled as composite material, where steel belts and radial plies are embedded in rubber components. The rubber is modeled as hyperelastic material to capture its incompressibility and nonlinearity, while the belt reinforcement is modelled as linear elastic material with high modulus (Hernandez and Al-Qadi 2016, Ding and Wang 2016; 2017).

The development of the tire models includes the following steps: (1) apply internal inflation pressure on the axisymmetric tire models; (2) establish surface contact between the tire and rim, and the tire and pavement surface; (3) simulate tire static deflection by giving the road surface a given displacement to reach the tire rated load; (4) simulate tire rolling at the specific travelling and rotation speed. By comparing the predicted tire deflections for different mesh sizes, the final mesh was determined until the changes in the result was smaller than 5%. The length of elements in the tire contact patch was selected to be 6 to 11mm; while the width of element varies from 5 to 8mm. Figure 2 presents the 2-D and 3-D meshes of truck tire models used in the analysis.

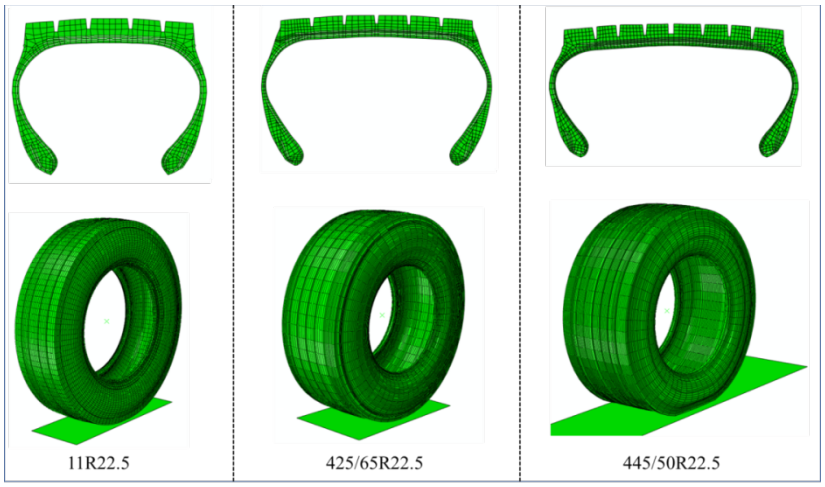

Figure 2 Truck tire models used in the analysis.

2.2 Validation of tire model with tire deflections

Tire deflection is an important measure of the tire stiffness in response to the vertical load. In this paper, measured tire deflections provided by tire manufactures were used to calibrate tire material parameters used in the models (Wang et al. 2012). The calculated deflection showed good agreements with the measured data, as illustrated in Figure 3. The good agreements between the measured and calculated tire deflections indicate that the proposed tire model is adequate for tire-pavement interaction analysis.

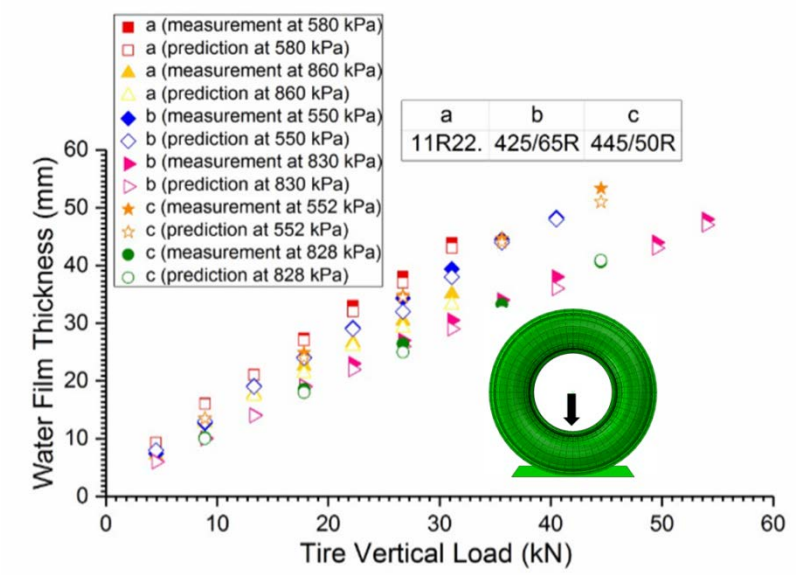

Figure 3 Comparisons between measured and predicted deflections.

Section 3: Fluid-Structure interaction models

3.1 Fluid Domains

Numerical modelling of fluid-structure interaction often involves discretization of multidimensional domains into finite elements. Each element satisfies the relevant governing equations of the kinematics of the continuum. Consider a Cartesian coordinate system (x, y, z), ∇ is defined as

$$\nabla = \left[\frac{\partial}{\partial x}, \frac{\partial}{\partial y}, \frac{\partial}{\partial z} \right] \tag{1}$$

In this study, the fluids (water and air) are treated as Newtonian fluid (viscosity is constant) and the temperature change of water is negligible. For incompressible flows, the flow velocity V is governed by the continuity equation

$$\nabla \cdot V = 0 \tag{2}$$

And the conservation of momentum

$$\rho \left(\frac{\partial V}{\partial t} + V \cdot \nabla V \right) = \nabla \cdot \sigma + \rho g \tag{3}$$

For Newtonian fluid, the fluid stress tensor

$$\sigma = -(p + \frac{2}{3} u(\nabla \cdot V)) I + 2uD \tag{4}$$

And rate of deformation tensor

$$D = \frac{1}{2}((\nabla V) + (\nabla V)^T) \tag{5}$$

Substitute Eq. (2), Eq. (4) and Eq. (5) into Eq. (3), the incompressible Navier-Stokes Equation for hydroplaning becomes

$$\rho(\frac{\partial V}{\partial t} + V \cdot \nabla V) = -\nabla p + u\nabla^2 V + \rho g \tag{6}$$

with boundary conditions given by

$$\hat{u} \cdot n = \hat{u}_s \text{ on } S_{\hat{u}} \tag{7}$$

$$\hat{u} \cdot t = \hat{u}_t \text{ on } S_{\hat{u}} \tag{8}$$

In above equations, ρ is water density, g is body accelerations, p is pressure, u is dynamic viscosity, I is identity matrix, $(\nabla \cdot)$ is the divergence operator, $(\cdot)$ is the internal product, ∇V is the gradient of the velocity field, $S_{\hat{u}}$ corresponds to the part of the surface with imposed displacements $\hat{u}_s$ and $\hat{u}_t$ in the normal and tangential directions respectively. n and t are unit normal and tangent vectors to the boundary, and $\hat{u}$ is the boundary displacement.

3.2 Solid Domains

To model the behaviour of structure system the Lagrangian formulation of motion is employed. The Lagrangian equations of motion of the structure are

$$\rho \frac{\partial^2 u}{\partial t^2} = \nabla \cdot \tau + f^B \tag{9}$$

where ρ is the density, u represents the vector of structural displacements, t is the time, τ is the Cauchy stress tensor, and f^B denotes the vector of body forces, and ($\nabla\cdot$) is the divergence operator in the deformed configuration.

with boundary conditions given by

$$u = u_s \quad \text{on } S_u \tag{10}$$

$$\tau \cdot n = f^S \quad \text{on } S_f \tag{11}$$

where S_u and S_f denote the boundaries with prescribed displacements u_s, and tractions f^S, respectively; and n is a unite outward normal vector to the boundary.

3.3 Coupling of the Equations for Fluid and Structure

While the spatial discretization of the fluid domain is based on the finite volume formulation using Eulerian coordinates, the solid domain consists of finite elements in a Lagrangian description. The meshes from two domains do not match since both models have different discretization and do not have to share the same grid points. The coupled method enables independent discretization and refinement of the areas of physical interests. Equations (6) and (9) can be discretized using the finite element method and can be coupled by the following fluid-structure interfacial boundary conditions (*Rugonyi and Bathe 2001*).

$$\tau^S \cdot n = \tau^F \cdot n \tag{12}$$

$$u^I(t) = \hat{u}^I(t) \tag{13}$$

$$\dot{u}^I(t) = v^I(t) = \hat{v}^I(t) \tag{14}$$

$$\ddot{u}^I(t) = \dot{v}^I(t) = \dot{\hat{v}}^I(t) \tag{15}$$

Where, n is a unit vector normal to the fluid-structure interface, u is the displacement of the structure, $\hat{u}$ is the displacement of the fluid domain, v and $\hat{v}$ are the velocities of the fluid and the fluid domain, respectively. S, F and I represent the solid, the fluid media and the fluid-structure interface, respectively.

Section 4: Hydroplaning Model

4.1 Tire Hydroplaning Model

In hydroplaning analysis, the fluid is treated as incompressible, isotropic and Newtonian fluid with a constant viscosity. The body force is considered in the simulation in addition to the applied tire load. The hydroplaning analysis is conducted in a moving frame of reference, in which the water and road surface are moving toward the tire structure at a given speed, and the tire rolls at a fixed location with angular velocity.

In this study, the Coupled Eulerian-Lagrangian (CEL) method is used to capture the hydroplaning phenomenon. With CEL, the flowing fluid can be modelled effectively using Eulerian analysis and the tire structure can be treated using traditional nonlinear Lagrangian analyses. In the CEL method, material is tracked as it flows through the mesh by computing its Eulerian volume fraction within each element (Cho *et al. 2006*). By defining the Eulerian elements initially, into which water is expected to later move, the free surface of the fluid can be simulated and this enables the analysis of water scattering drained by tread patterns.

In the current study, the volume fraction of water to track the flow boundary is expressed by $F(x;t) \in [0,1]$, as shown in Equation 16,

$$\frac{\partial F}{\partial t} + V \cdot \nabla F = 0 \qquad (16)$$

In the CEL method, if the element is fully filled with water, its volume fraction $F = 1$; if no water is present in an element, then the volume fraction $F = 0$. In the tire hydroplaning simulation, both water and air voids are treated as Eulerian elements. If the sum of all material volume fractions in an element is less than one, i.e. $0 < F < 1$, the air void will automatically fill the remainder of the element.

An example of Eulerian mesh is presented in Figure 4. The dimension of the fluid domain should be large enough to enclose the entire trajectory of interest, for example, the tire contact patch. In this study, the fluid domain has a width of 560 mm, length of 548 mm, and the depth of air above water is fixed at 50 mm. The element size of the water layer should be less than or equal to the tire groove width. However, if the entire region of the water domain is adapted with finer meshes, the total number of elements becomes huge and the computation time increases drastically. Sensitivity analysis showed that the element size of the fluids at the contact patch should be smaller than one half of the groove width in the tread to obtain reasonable accuracy. In order to obtain sufficient numerical accuracy and efficiency, the fluid domain around the tire contact patch where the deformed tire and fluid interface is equally divided into small size meshes with element length of 1.0 mm. In other regions away from the tire contact zone, the sizes of element length are 10 mm.

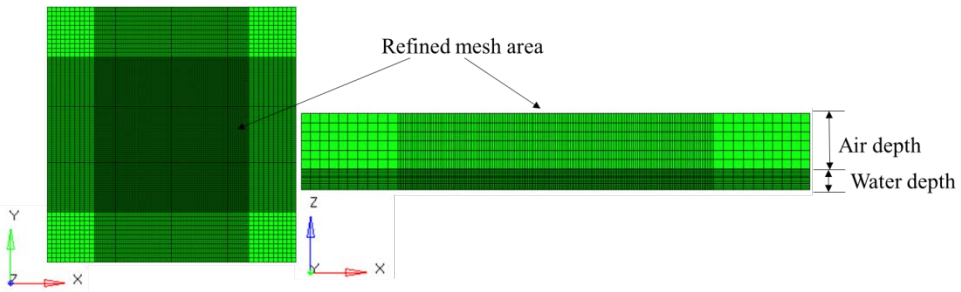

Figure 4 Mesh configuration of fluid model.

The boundary conditions of the fluid domain include inlet velocity at the front of the fluid domain to simulate vehicle speed; and moving wall boundary condition for water and pavement interface. Figure 5 shows the fluid-structure interaction model for hydroplaning simulation. In this study, the criteria used for judging hydroplaning is when the contact force at tire-pavement contact patch is zero (the water uplift force is equal to the vertical load on tire).

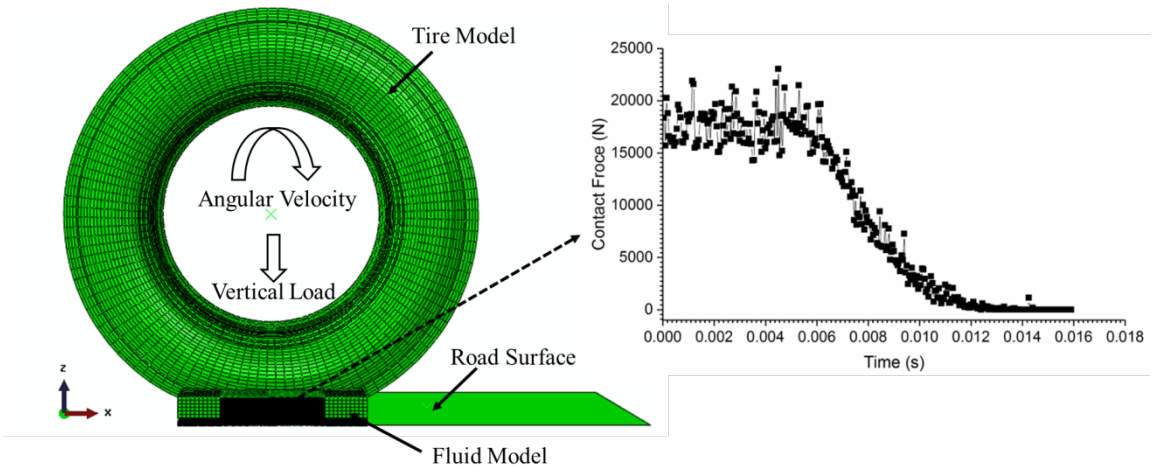

Figure 5 Truck tire hydroplaning model with contact force variation.

4.2 Validation of Hydroplaning Model

There are many empirical equations that have been developed to predict the hydroplaning speed. However, these existing empirical models are often limited to a certain type of tire or water film depth. For example, the TXDOT equation developed by Gallaway (1979) is based on specific tire profiles. The NASA hydroplaning equation has been widely used to predict hydroplaning speed of passenger car tires on wet pavements. However, field observations and experimental studies have found that these equations cannot describe the hydroplaning behaviour of commercial truck tires (Ong and Fwa 2008).

Horne et al. (1986) conducted a series of tests on worn bias-ply truck tries under vertical loads up to 4200 N at various tire inflation pressure levels. Based on the test data, the predictive equation for hydroplaning speed was proposed, as shown in Equation 17. However, the equation is limited to a certain type of bias-ply tire and the hydroplaning speed is only dependent on tire inflation pressure and footprint aspect ratio, neglecting the effect of water film thickness and tire operating conditions.

$$v_p = 25(p_t)^{0.21}(\frac{1.4}{FAR})^{0.5} \qquad (17)$$

Where, v_p is the hydroplaning speed in km/h, p_t is the tire inflation pressure in kPa, and FAR is the footprint aspect ratio (width of tire contact patch over its length).

Due to the above-mentioned limitations of empirical equations, the results from experimental tests conducted by Texas Transportation Institute were used to validate

the proposed hydroplaning model (Tielking 1992). The hydroplaning tests were conducted by towing a single test tire on the wet surface that is 244 m long and 0.8 m wide. The water depth was kept at 19 mm to allow tire grooves completely flooded. The wide-base 425/65R22.5 and conventional 11R22.5 tires were tested with 690 kpa inflation pressure and different tire loads. The tire hydroplaning was detected by an abrupt spin-up when the test tire exits onto dry pavement. The measured and predicted hydroplaning speeds were presented in Table 2. As the results show, good agreements were observed between the hydroplaning speeds predicted from the proposed model in the current study and the measurement results. This indicates that the proposed model can be used to predict hydroplaning speed with acceptable accuracy.

Table 2 Hydroplaning Speeds for 425/65R22.5 and 11R22.5 Tires

Type of Truck Tire	Tire Load (kN)	Measured Hydroplaning Speed (Tielking 1992) (km/h)	Predicted Hydroplaning Speed (km/h)	Difference (%)
425/65R22.5	11.1	90.7	87	-4.0
	17.8	100.4	96	-4.4
11R22.5	8.9	84.5	79	-6.5
	22.2	94.7	90	-4.9

Section 5: Results and Discussions

5.1 Effect of tire configuration on hydroplaning

This subsection studies the effect of tire configuration on hydroplaning. The simulation was performed for two different wide-base tires (425 and 445) and the single 11R22.5 tire at tire inflation pressure of 690 kPa, respectively. The tire load applied on the single 11R22.5 tire and wide-base tire is 8.9 kN and 17.8 kN, respectively. This is based on the assumption that the dual tire assembly will carry the same load as the wide-base tire. The water film thickness on pavement surface is fixed at 19 mm.

Figure 6 presents the contour plots of tire contact patches at tire speed of 96 km/h, respectively, for three different tires. The output variable EVF_WATER denotes the volume fraction for water. In the contour plot, the areas occupied by water (EVF=1) appear as red colour as shown in the top of contour spectrum, while the areas unoccupied by air (EVF=0) appear as blue colour as shown in the bottom of contour spectrum. The boundary between the dry and wet areas is the transition area. The white colour indicates the tire contact patch at the tire-pavement interface. It is can be seen that at t=0.004 second, all three tires have full contact with the road surface. At t=0.006 second, when the water interacts with the tire, water begins to occupy the tire contact patch. The contact patch gets smaller as the water flow into the tire grooves becomes prominent at t=0.008 second. At the same time, the rainwater starts to drain from the left and right sides of tire in addition to water flow in the grooves.

Figure 7 shows the tire-pavement contact forces of three tires in the vertical direction during the process of hydroplaning. At t=0.008 seconds, the tire-pavement contact force of 11R22.5 tire decreases to zero. This indicates that the hydrodynamic force provided by water reaches to a certain level that is high enough to lift the tire, which causes the tire to lose contact with road surface and hydroplaning. However, for the wide-base 425 and 445 tires, the tire still has partial contact with road surface. The simulation results indicated the 11R22.5 tire is more prone to hydroplaning as compared to wide-base tires and the wide-base 445 tire has the highest hydroplaning speed.

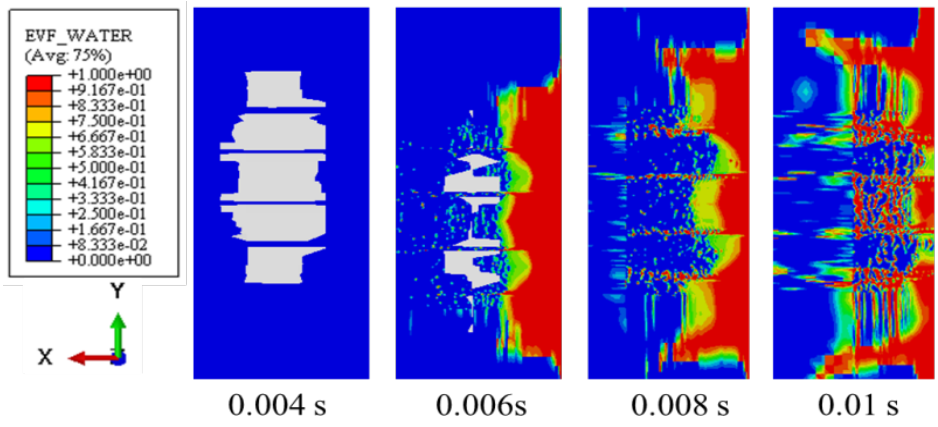

(a)

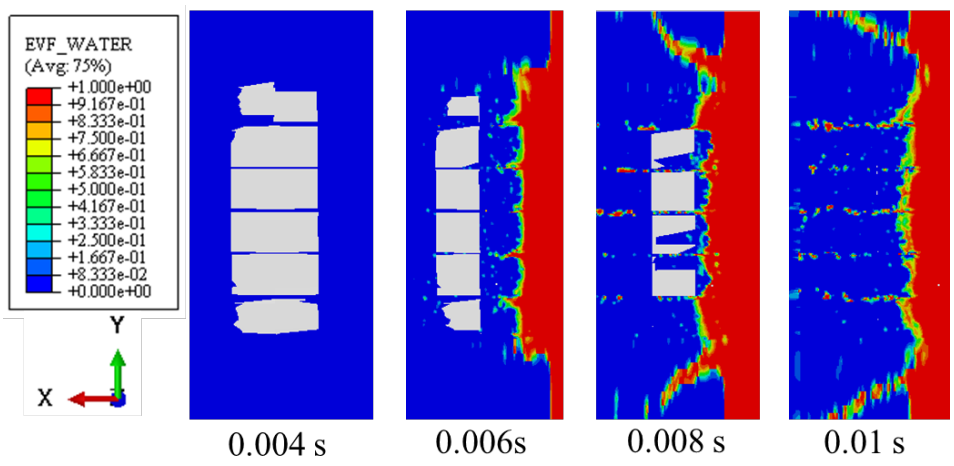

(b)

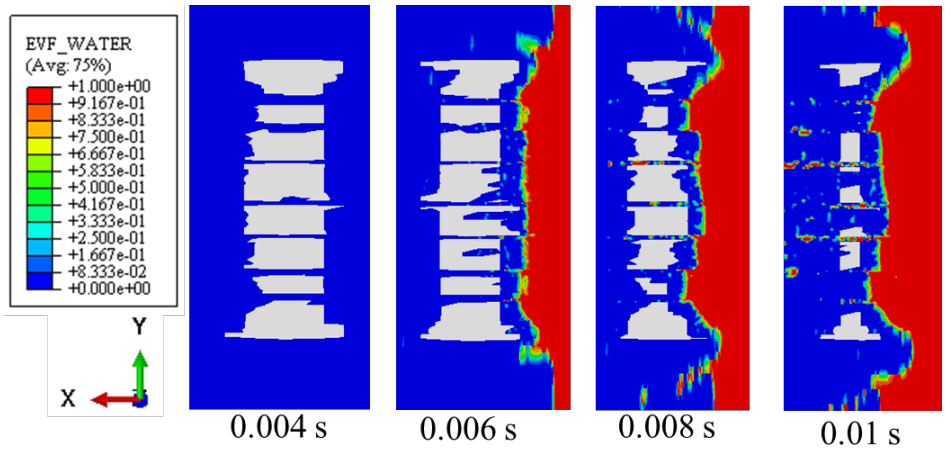

(c)

Figure 6 Illustration of water flow into tire contact patch for (a) single 11R22.5 tire, (b) wide-base 425 tire, and (c) wide-base 445 tire at 96 km/h.

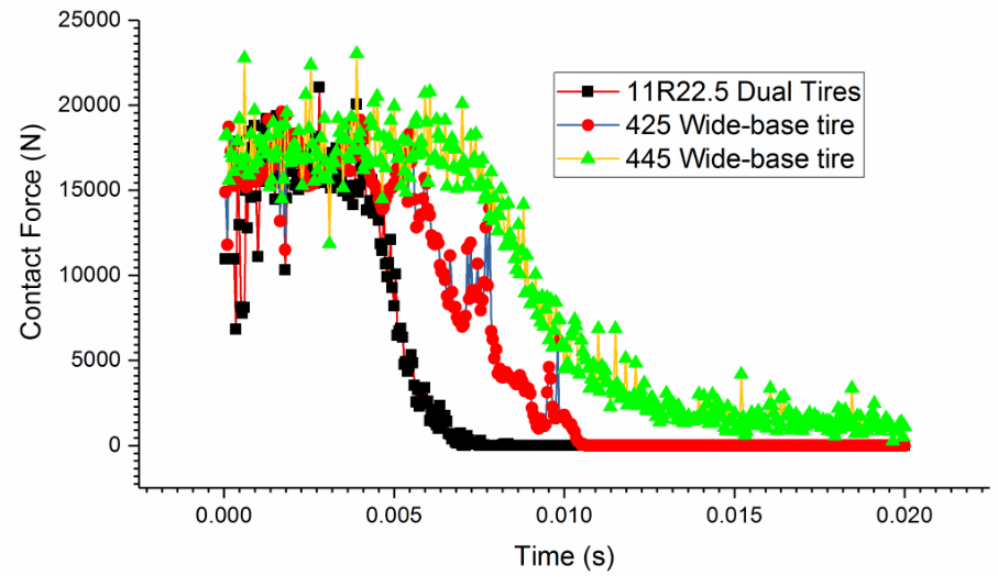

Figure 7 Tire-pavement contact force variation during hydroplaning process.

5.2 Effect of water film thickness on hydroplaning

There are several empirical equations that can be used to compute the water film thickness (Gallaway *et al*. 1971, Anderson *et al*. 1998). In general, these models share lots of similarities, in which the input parameters typically include pavement texture, rainfall intensity, pavement slope, drainage path, and, in some cases, Manning's roughness coefficient. The model developed by Anderson et al. (1998) has been widely used to predict water film thickness on highway pavement due to its simplicity and ease of implementation. The model is presented in Eq. 18. Figure 8 presents the change of water film thickness with the drainage path length as the slope of drainage path is assumed at 2%.

$$WFT = \left(\frac{n \times L \times r}{36.1 \times S^{0.5}} \right)^{0.6} - MTD \tag{18}$$

Where, *WFT* is water film thickness (in.); *n* is Manning's roughness coefficient; *L* = drainage path length (in.); *r* is excess rainfall rate (in./h) that is equal to the difference between rainfall rate and infiltration rate (permeability of pavement); *S* is slope of drainage path (in./in.); and *MTD* is mean texture depth (in.).

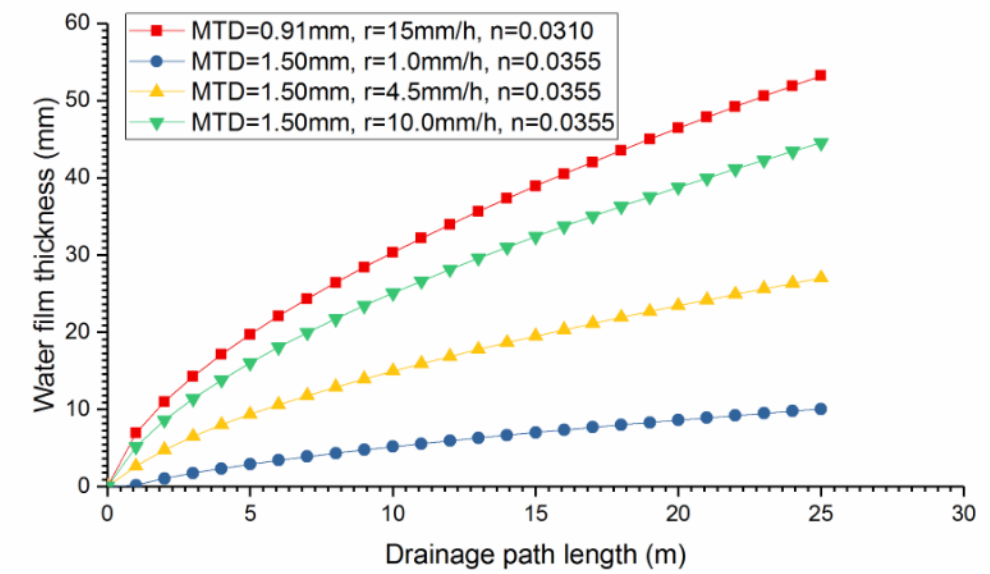

Figure 8 Water film thicknesses along drainage path length at different conditions.

The variation of hydroplaning speeds or wide-base 425 and 445 tires at different water film thicknesses is presented in Figure 9. The simulations were performed for 425 and 445 wide-base tires under loading of 17.8 kN with tire inflation pressure of 690 kPa. At the constant tire vertical load and inflation pressure, it can be observed that the hydroplaning potential increases for both tires as the water film depth increases. The results clearly show that wide-base 445 tire shows the higher hydroplaning speed than wide-base 425 tire. For example, at heavy rain rate with water film thickness of 41 mm,

the hydroplaning speed of wide-base 445 tire is 88 km/h, which is 11.4% higher than that of wide-base 425 tire. This is because the wide-base 445 tire has two more grooves and the deeper tread depth as compared to the wide-base 425 tire.

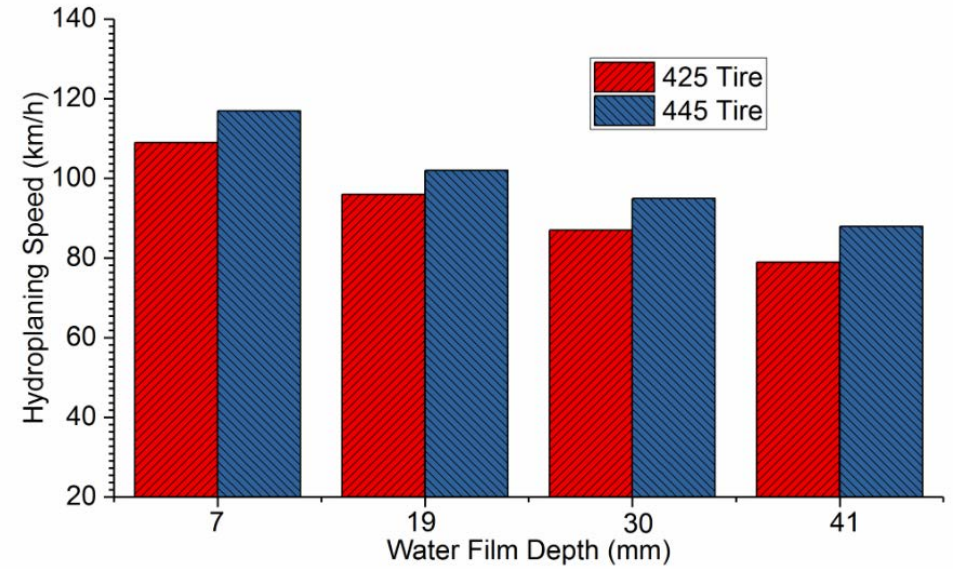

Figure 9 Effect of water film thickness on hydroplaning speed.

5.3 Effect of wheel load on hydroplaning

In this section, four typical loads were selected for analysis, including 11.1 kN, 17.8 kN, 26.7 kN and 44.5 kN. The hydroplaning simulation was performed for two wide-base tires with water film depth of 19 mm and tire inflation pressure of 690 kPa. Figure 10 shows the variation of hydroplaning speeds with wheel loads. The results indicate the positive influence of wheel load on hydroplaning speed. For example, for the light trucks with 11.1-kN load on tire, the hydroplaning speeds of wide-base 425 and 445 tires are 87 km/h and 96 km/h, respectively. As the load increases to 44.5 kN, the hydroplaning speeds are 113 km/h and 120 km/h, respectively. The higher

hydroplaning speed can be attributed to the wider and deeper groove size of 445 tire compared with 425 tire. The positive influence of grooved width and depth on hydroplaning speed are also supported by other researchers (Fwa 2009, Kumar 2010).

Figure 11 presents the illustration of water penetration into tire contact patch at various vertical load for 445 tire (t=0.01s). It is obvious that at smaller vertical load, the tire loses contact with the road surface quicker, which indicates that the empty trucks are more prone to experience hydroplaning.

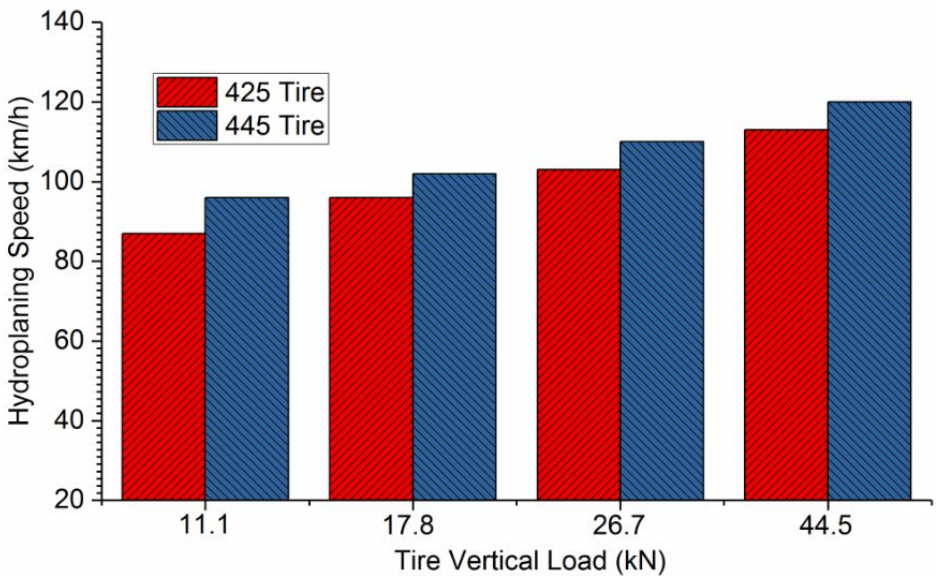

Figure 10 Effect of wheel load on hydroplaning speed.

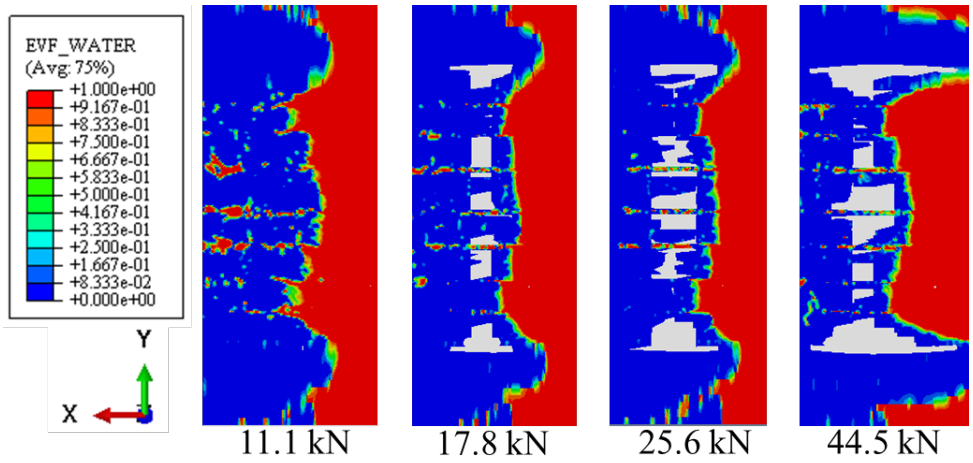

Figure 11 Illustration of water penetration into tire contact patch at various vertical load for wide-base 445 tire.

5.4 Effect of tire inflation pressure on hydroplaning

Truck using different tire configurations may operate at different levels of tire inflation pressure. Hydroplaning simulations were conducted at three tire inflation pressure levels of 550 kPa, 690 kPa and 830 kPa under the same load of 17.8 kN. The water film thickness is fixed at 19 mm.

The simulation results for two wide-base tires are shown in Figure 12. The results show that hydroplaning speed increases with the increase of tire inflation pressure at constant tire load. For example, the hydroplaning speeds are 88 km/h and 93 km/h at inflation pressure of 550 kPa, respectively, for wide-base 425 and 445 tires, while the hydroplaning speeds increase to 102 km/h and 110 km/h when the inflation pressure increases to 830 kPa. This indicates that underinflated tires are more prone to

hydroplane during wet weather. The reason can be attributed to the change of tire-pavement contact behaviour as tire inflation pressure changes (Wang and Al-Qadi 2012).

Figure 13 shows the illustration of water penetration into tire contact patch at different inflation pressure level. A tire with lower inflation pressure has larger contact area and the smaller peak contact stress under tire canter, which may cause water penetration into tire contact patch more easily. On the other hand, the higher tire inflation pressure causes the smaller contact area but the higher peak contact stress. Therefore, the high tire inflation pressure increases the resistance of water flowing into the tire contact patch.

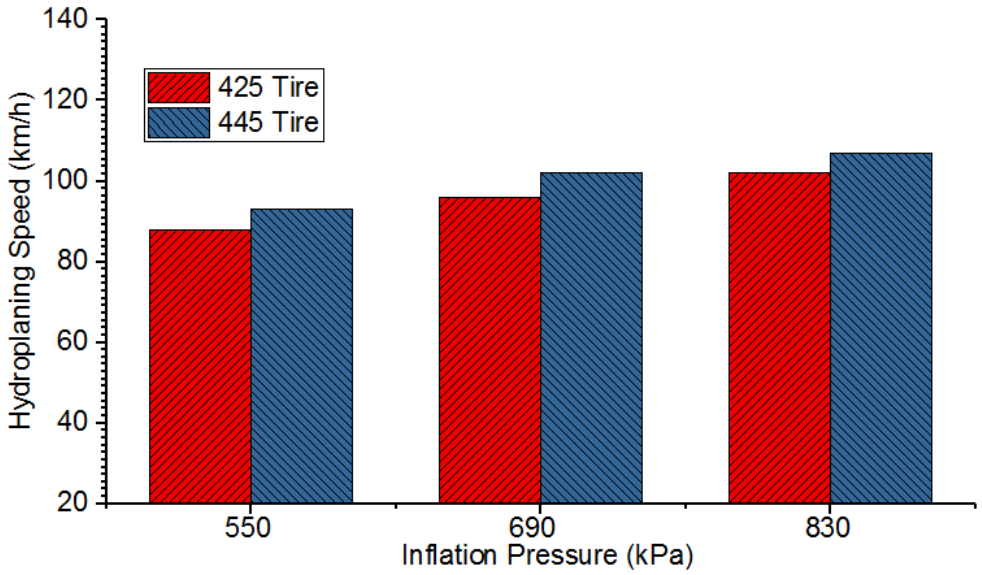

Figure 12 Effect of tire inflation pressure on hydroplaning speed.

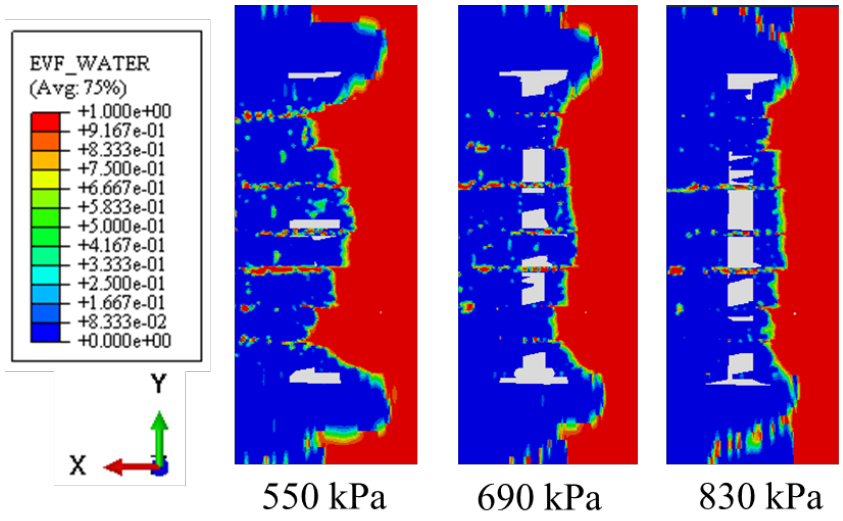

Figure 13 Illustration of water penetration into tire contact patch at various tire pressure levels for wide-base 445 tire.

5.5 Effect of tire sliding on hydroplaning

When vehicles travel on roadway with different operation conditions, tires have different rolling conditions, such as free rolling and sliding. In previous sections, the hydroplaning phenomena under free rolling condition were analysed. In this subsection, the hydroplaning speeds for wide-base 445 tire under the locked-wheel condition (sliding) were compared with the ones under free rolling condition. A constant water film depth of 19 mm and wheel load of 17.8 kN are considered in the simulation.

The comparison of hydroplaning speeds under free rolling and sliding condition is presented in Figure 14. The results show that the hydroplaning speeds of free-rolling tire is 3-6 km/h higher than those of fully-locked sliding tire depending on tire inflation pressure. Previous research has reported that the hydroplaning speeds of passenger car

tires decrease by 4-16.5 km/h as the tire changed from free rolling to sliding condition (Kumar et al. 2012). This indicates that hydroplaning speed of truck tire is less sensitive to tire slippage as compared to passenger car tire, which is probably due to the relatively heavy load and high tire pressure.

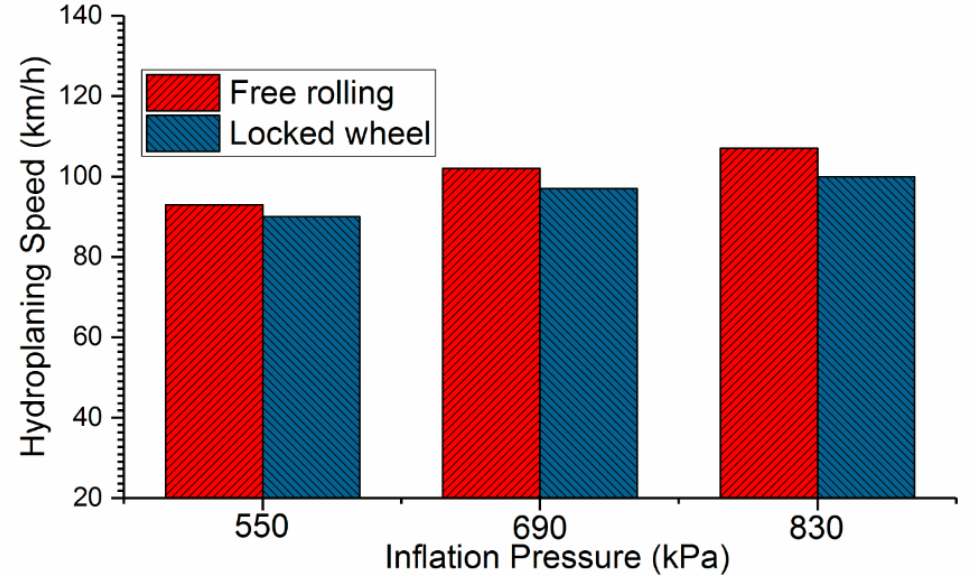

Figure 14 Hydroplaning speeds of wide-base 445 tire under free rolling and locked-wheel conditions.

The influence of tire slippage on hydroplaning can be attributed to the relative speed of tire and water is greater when tire is sliding in the direction opposite to water flow, as compared to tire rotation along the direction of water flow. The relative movement of tire to water flow affects the amount of water pushed into tire contact patch when tire rolls on flooded pavement surface. As can be seen from Figure 15, the drainage capacity of the side grooves under sliding condition is reduced, which results in more water

accumulation at the tire edge. Thus, it is more difficult for the entrapped water to escape beneath a sliding tire as compared to a rolling tire. However, under free rolling condition, water can be more easily escaped through the grooves, and there is less entrapped water at tire edge, which delays the occurrence of hydroplaning.

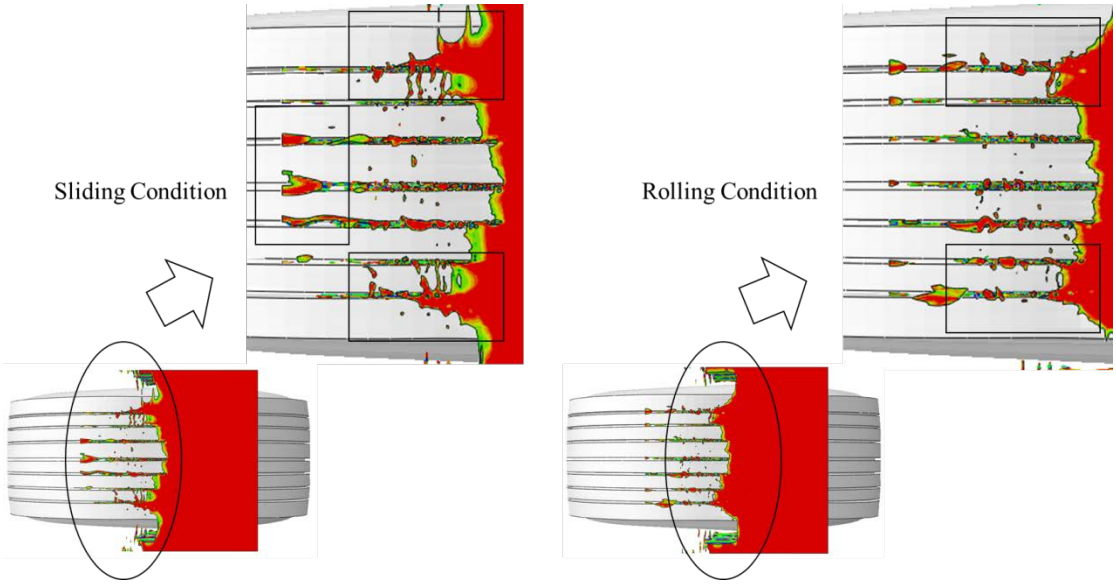

Figure 15 Illustration of water flow into contact patch of wide-base 445 tire under free rolling and sliding conditions.

5.6 Conclusions

In this study, tire hydroplaning models based on 3D fluid-structure interaction were developed to analyse hydroplaning speeds of three truck tire configurations at different conditions. The fluid-structure interaction model was validated with measured tire hydroplaning speeds from previous study. The results show that the wide-base 445 tire provides better safety performance than the conventional wide-base 425 tire and dual tire assembly with 11R22.5 tire under wet weather condition.

The hydroplaning potential increases with the increase of water film thickness on pavement surface. On the other hand, the high wheel load or high tire inflation pressure positively increases hydroplaning speed. The differences in the hydroplaning speed were found to be 5 to 9 km/h at different wheel loads, tire inflation pressure levels, and water film thicknesses. In addition, the analysis results demonstrate that the truck tire under sliding condition has the greater hydroplaning risks than the tire under free rolling condition.

The findings indicate that tire hydroplaning on flooded pavement surface is highly related to tire configurations and operating conditions in addition to water film depth on pavement surface that is more affected by roadway geometric factors. These factors should be considered together when developing safety improvement countermeasures for driving safety.

References

Anderson, D. A., Huebner, R. S., Reed, J. R., Warner, J. C., and Henry, J. J., 1998. *Improved Surface Drainage of Pavement: Final Report*. Transportation Research Board, The National Academies Press.

Al-Qadi, I.L., and Elseifi, M.A. 2007. New Generation of Wide-Base Tires: Impact on Trucking Operations, Environment, and Pavements, *Transportation Research Record: Journal of the Transportation Research Board*, 2008,100–109.

Al-Qadi, I.L., and Wang, H. 2012 Impact of Wide-Base Tires on Pavements: Results from Instrumentation Measurements and Modelling Analysis, *Transportation Research Record: Journal of the Transportation Research Board*, 2304, 169–176.

ABAQUS, 2010. *Analysis User's Manual*. Abaqus, Version 6.10–EF.

Cho, J. R., Lee, H. W., Sohn, J. S., Kim, G. J., and Woo. J. S., 2006. Numerical Investigation of Hydroplaning Characteristics of Three-Dimensional Patterned Tire. *European Journal of Mechanics-A/Solids*, 25, 914–926.

Ding, Y. M., and Wang, H., 2016. BEM-FEM Model for Truck Tire-Pavement Interaction Noise Prediction. *Tire Science and Technology*, 44, 212–224.

Ding, Y. M., and Wang, H., 2017. FEM-BEM analysis of tyre-pavement noise on porous asphalt surfaces with different textures. *International Journal of Pavement Engineering*, 1–8.

Fwa, T. F., and Ong, G. P., 2007. Wet-Pavement Hydroplaning Risk and Skid Resistance: Analysis. *Journal of Transportation Engineering*, 134(5), 184–190.

Fwa, T.F., Kumar, S. S., and Anupam. K., 2009. Effectiveness of Tire-Tread Patterns in Reducing the Risk of Hydroplaning, *Transportation Research Record: Journal of the Transportation Research Board*, 2094, 91–102.

Gallaway, B. M., Schiller, R. E., and Rose, J. G., 1971. *The Effects of Rainfall Intensity, Pavement Cross Slope, Surface Texture and Drainage Length on Pavement Water Depths*. College Station, Texas: Texas Transportation Institute.

Gallaway, B. M., 1979. *Pavement and Geometric Design Criteria for Minimizing Hydroplaning*. Publication FHWA-RD-79-31. FHWA, U.S. Department of Transportation.

Harrin, E. N., 1958. *Low Tire Friction and Cornering Forces on a Wet Surface*. NACA Technical Notes NACA-TN-4406, NACA, National Advisory Committee for Aeronautics.

Horne, W. B., and Dreher, R. C., 1963. *Phenomena of Pneumatic Tire Hydroplaning*. NASA Technical Note D-2056, NASA, National Aeronautics and Space Administration.

Horne, W. B., Yager, T. J. and Ivey, D. L., 1986. Recent Studies to Investigate Effects of Tire Footprint Ratio on Dynamic Hydroplaning Speed. *The Tire Pavement Interface,* Special Technical Publication 929, ASTM International, West Conshohocken, PA, 26–46.

Ivey, D.L., 1984. *Truck Tire Hydroplaning-Empirical Verification of Horne's Thesis*. Presentation to the Technical Seminar on Tire Service and Evaluation, ASTM Committee F-9, November, Akron, Ohio, USA.

Ong, G.P., Fwa, T. F. and Guo, J., 2005. Modeling Hydroplaning and the Effects of Pavement Micro-Texture. *Transportation Research Record: Journal of the Transportation Research Board,* 1905, 166–176.

Ong, G. and Fwa, T. F., 2008. Modeling and analysis of truck hydroplaning on highways, *Transportation Research Record: Journal of the Transportation Research Board*, 2068, 99–108.

Rugonyi, S., and Bathe, K. J., 2001. On Finite Element Analysis of Fluid Flows Fully Coupled with Structural Interactions. Computer Modeling in Engineering and Sciences, 2, 195–212.

Stocker, A. J., Dotson, J.T., and Ivey, D.L., 1974. *Automobile tire hydroplaning-A study of wheel spin-sown and other variables*, Research Report, Texas Transportation Institute Texas A&M University College Station, Texas.

Sinnamon, J. F. 1974. *Hydroplaning and Tread Pattern Hydrodynamics*, Publication UM-HSRI-PF-74-10. Highway Safety Research Institute, the University of Michigan.

Tielking, J. T. 1992. *Conventional and Wide Base Radial Truck Tyres. Proceedings of the Third International Symposium on Heavy Vehicle Weights and Dimensions*, Queen's College Cambridge, UK, 182–190.

Veith, A.G. 1983. Tires-Roads-Rainfall-Vehicles: The Traction Connection. Frictional Interaction of Tire and Pavement, Special Technical Publication 793, ASTM International, West Conshohocken, 3–30.

Wang, H., and Al-Qadi, I.L. 2011. Impact Quantification of Wide-base Tire Loading on Secondary Road Flexible Pavements, *Journal of Transportation Engineering*, 137, 630–639.

Wang, H., Al-Qadi, I.L., and Stanciulescu, I. 2012. Simulation of Tire-Pavement Interaction for Predicting Contact Stresses at Static and Various Rolling Conditions, *International Journal of Pavement Engineering*, 13, 310–321.

Kumar, S.S., Anupam, K., Scarpas, T., and Kasbergen, C. 2012, Study of Hydroplaning Risk on Rolling and Sliding Passenger Car, *Procedia - Social and Behavioral Sciences*, 53, 1020–1028.

Kumar, S.S., Anupam, K., and Fwa, T. F. 2010, Analyzing Effect of Tire Groove Patterns on Hydroplaning Speed, *Journal of the Eastern Asia Society for Transportation Studies*, 8, 1881–1124.